Role of Native-State Structure in Rubredoxin Native-State Hydrogen Exchange†

David M. LeMaster,‡ Janet S. Anderson,§ and Griselda Hernández*,‡

Wadsworth Center, New York State Department of Health, Empire State Plaza, Albany, New York 12201, and Department of Chemistry, Union College, Schenectady, New York 12308

Received March 20, 2006; Revised Manuscript Received June 25, 2006

ABSTRACT: Amide exchange rates were measured for *Pyrococcus furiosus* (*Pf*) rubredoxin substituted with either Zn(II), Ga(III), or Ge(IV). Base-catalyzed exchange rate constants increase up to 3000-fold per unit charge for the highly protected amides surrounding the active site metal, yielding apparent residue-specific conformational energy decreases of more than 8 kcal/mol in a comparison of the Zn(II)- and Ge(IV)-substituted proteins. However, the exchange kinetics for many of the other amides of the protein are insensitive to these metal substitutions. These differential rates are inversely correlated with the distance between the amide nitrogen and the metal in the X-ray structure, out to a distance of at least 12 Å, consistent with an electrostatic potential-dependent shifting of the amide nitrogen p*K*. This strongly correlated distance dependence is consistent with a nativelike structure for the exchange-competent conformations. The electric field potential within the interior of the rubredoxin structure gives rise to a change of as much as a million-fold in the rate for the exchange-competent state of the individual amide hydrogens. Nevertheless, the strength of these electrostatic interactions in *Pf* rubredoxin appears to be comparable to those previously reported within other proteins. As a result, contrary to the conventional analysis of hydrogen exchange data, for exchange processes that occur via nonglobal transitions, the residual conformational structure will often modulate the observed rates. Although this necessarily complicates the estimation of the conformational equilibria of these exchange-competent states, this dependence on residual structure can provide insight into the conformation of these transient states.

More than 50 years ago, before the first protein X-ray structure was reported, the hydrogen exchange experiments of Linderstrøm-Lang and co-workers (*1*) demonstrated that the conformation of a protein can strongly protect backbone amide protons from exchange with the hydrogens in the bulk water. However, exchange eventually did occur, thus first demonstrating the dynamic character of the protein structure. The kinetics of this process are generally represented according to the following equation:

$$\text{closed} \underset{k_2}{\overset{k_1}{\rightleftharpoons}} \text{open} \xrightarrow{k_3} \text{exchanged}$$

If the rate of the closing reaction is rapid compared to the rate of the "open"-state chemical exchange step (i.e., $k_2 \gg k_3$), a pre-equilibrium of the open and closed conformational states is established and the overall exchange rate constant equals $(k_1/k_2)k_3$, where k_1/k_2 is the equilibrium constant for the conformational opening transition. In her classic review of protein hydrogen exchange (*2*), Hvidt stated the central issue for the quantitative interpretation of hydrogen exchange rates in terms of conformational dynamics.

"If it [the exchange-competent conformation] is not fully exposed to the aqueous solvent, k_3 cannot be assumed to be known from studies of hydrogen exchange in aqueous solutions of oligopeptides and randomly coiled polypeptides, and few inferences concerning the values of k_1 and k_2 in reaction scheme can be made from observed rates of hydrogen exchange in proteins."

The assumption that the open-state exchange rate is independent of residual conformational structure or equivalently that normalization against model peptide exchange data yields thermodynamic measurement of the open-state conformational equilibria (*3*) forms the core of the so-called "local unfolding" model. Conversely, the expectation that residual conformational structure in the exchange-competent state may potentially influence the rate of exchange from that state (*4*) came to be known as the "solvent penetration" model.

Amide hydrogens that exchange with bulk solvent via a global unfolding transition provide a condition for which the applicability of the peptide normalization assumption can be directly tested. Although exceptions have been noted (*5*−*10*), the most slowly exchanging amides for a number of proteins predict free energies of conformational stability similar to those independently obtained by standard reversible unfolding measurements (*11*). On the other hand, in all proteins, the great majority of amides exchange more rapidly than a global unfolding mechanism predicts.

Measurement of the relative exchange rates for a protein in a crystal and in solution (*12*, *13*), the correlation between depth of burial and exchange rate (*14*, *15*), denaturant concentration (*5*, *16*), and pressure (*17*) dependence of exchange have all been interpreted according to whether solvent penetration or a local unfolding transition provides

† This work was supported in part by NIH Grant GM 64736 (G.H.).

* To whom correspondence should be addressed. E-mail: griselda@wadsworth.org. Telephone: (518) 474-4673. Fax: (518) 473-2900.

‡ New York State Department of Health.

§ Union College.

10.1021/bi0605540 CCC: $33.50
Published on Web 07/27/2006

a more intuitive representation of the exchange-competent open state. However, none of these experiments directly probe the underlying question of whether the residual conformational structure modulates the exchange kinetics from this exchange-competent state.

To gain further insight into these nonglobal exchange processes, amide exchange kinetics can be measured as a function of varying sample conditions [e.g., temperature, denaturant, pressure, or pH (*18*)], a protocol denoted as native-state hydrogen exchange (*19*). The set of amides for which the exchange kinetics vary similarly as a function of the altered condition potentially indicates the spatial distribution of collective conformational transitions. Varying the charge of an active site metal provides a physiologically relevant means of modulating the conformational stability of a protein. Considering the simple Fe(II)−Fe(III) redox couple, the oxidized and reduced protein, in both the native and reversibly unfolded forms, define a closed four-state thermodynamic cycle. The free energy difference for the protein redox reaction in the native state versus that in the reversibly unfolded state is necessarily equal to the difference in the native-state conformational stability for the oxidized versus reduced forms. Thus, the redox-induced change in hydrogen exchange rates that is due to the differential global stability can potentially be separated from the contribution arising from the long-range electric field potential effect on the ionization step in the chemical exchange transition.

MATERIALS AND METHODS

Protein Purification and Metal Reconstitution. Uniformly ^{15}N enriched Zn(II)-substituted *Pyrococcus furiosus* (*Pf*) A2K rubredoxin was expressed and purified as previously described (*20*, *21*). Zn^{2+} was efficiently incorporated into rubredoxin during growth in a minimal medium containing 25 mg/L $ZnCl_2$. The Ga^{3+} and Ge^{4+} substitutions were carried out via reconstitution from metal-free protein. Uniformly ^{15}N enriched Fe(III)-substituted *Pf* A2K rubredoxin was expressed and purified as described for the Zn(II)-substituted protein with 10 mg/L $FeSO_4$ instead of $ZnCl_2$ in the growth medium. The apoprotein was prepared by precipitation with cold trichloroacetic acid to a final concentration of 20%. Aporubredoxin was then reconstituted at pH 8 with a final concentration of 2 mM $Ga(NO_3)_3$ or 0.2% $Ge(OEt)_4$, analogous to the protocol used for the previously described metal reconstitution studies of rubredoxin (*22*, *23*).

Hydrogen Exchange Measurements. Aliquots of the protein samples were dialyzed against buffers containing 100 mM sodium chloride and either 20 mM sodium succinate, 20 mM sodium phosphate, or 20 mM sodium borate in which the pH was adjusted to 4.5, 5.5, 6.5, 7.5, and 8.5 [only up to pH 7.5 for the Ge(IV)-substituted *Pf* A2K rubredoxin]. The protein samples (400 μL) were then lyophilized. The exchange experiments were initiated by quickly redissolving the samples in an equivalent volume of ^2H_2O and beginning the NMR data collection at 23 °C. The pH value of the samples were determined during acquisition by monitoring fast carbon acid exchange (D. M. LeMaster, J. S. Anderson, and G. Hernández, manuscript in preparation). For each sample, between 30 and 35 ^{1}H−^{15}N two-dimensional FHSQC (*24*) spectra were collected on a Bruker DRX 500 spectrometer over the course of several months to more than a year, depending on the resonances being monitored at the given pH. The data were processed with FELIX (Accelerys, San Diego, CA) using cosine bell weighting functions. The time courses of the amide peak intensities were fitted to exponential decays.

RESULTS

Apparent Residue-Specific Conformational Free Energy. Rubredoxin is the simplest of the iron−sulfur proteins, bearing a single metal coordinated by four cysteine thiolates in an approximately tetrahedral arrangement. Substitution of the diamagnetic Zn^{2+} ion provides an accurate structural mimic of the Fe(II)-substituted rubredoxin (*25*), and zinc has been commonly used to eliminate the paramagnetic shifting and broadening of the NMR resonances observed for the Fe(II) and Fe(III) proteins (*20*, *26*−*29*). Similarly, the X-ray structures of the Fe(III)- and Ga(III)-substituted *Clostridium pasteurianum* (*Cp*) rubredoxin differ only slightly in C^α positions, sulfur−metal bond lengths, and sulfur−amide hydrogen bond lengths (rmsds of 0.13, 0.02, and 0.02 Å, respectively) (*23*). The transition from the Fe(II) to Fe(III) redox state of *Cp* rubredoxin yields a contraction in the average sulfur−metal bond distance (from 2.36 to 2.26 Å), while the sulfur−amide hydrogen bond lengths increase by 0.08 Å (*25*).

Recently, we (*30*) generated Ge(IV)-substituted rubredoxin, the first reported stable biomacromolecular coordination complex of this inorganic germanium ion. Substitution of Zn^{2+}, Ga^{3+}, and Ge^{4+} yields a series of rubredoxins that differ electronically solely by the charge of the metal nucleus. The four coordinating cysteine thiolate ions give rise to net charge states of −2, −1, and 0, respectively, for the metal coordination site with these three substitutions. Changing the charge of the metal site varies the electrostatic potential at each amide nitrogen in a distance-dependent manner. The resultant alteration of the p*K* value for each individual protein amide nitrogen, with the corresponding variation in chemical exchange rate constant k_3, can potentially indicate the effects of residual conformational structure in the exchange-competent state.

The rubredoxin from the hyperthermophilic archaeon *P. furiosus* is the most thermostable protein characterized to date (*21*, *28*). Mutation of Ala 2 of wild-type *Pf* rubredoxin to lysine (*Pf* A2K) yields the variant analyzed herein; its N-terminal interactions are similar to those of the mesophile *C. pasteurianum* homologue, but the variant retains nearly all of the thermal stability of the wild-type hyperthermophile protein. Although the rapid reversible unfolding transition of *Pf* A2K rubredoxin can be detected in the presence of much slower irreversible denaturation near its T_m of 137 °C (*21*), only the irreversible denaturation process is observed for the *Pf* and *Cp* rubredoxins under more typical thermal and denaturant conditions (*31*, *32*).

As a means of avoiding the complications of irreversible denaturation more generally, hydrogen exchange offers an approach to estimating differential conformational stabilities under conditions in which the native state is strongly favored. Several hydrogen exchange studies of the Zn(II)-substituted *Pf* rubredoxin have been previously reported (*20*, *28*, *29*). In our study, a parallel set of measurements were carried out on ^{15}N-enriched samples of Zn(II)-, Ga(III)-, and

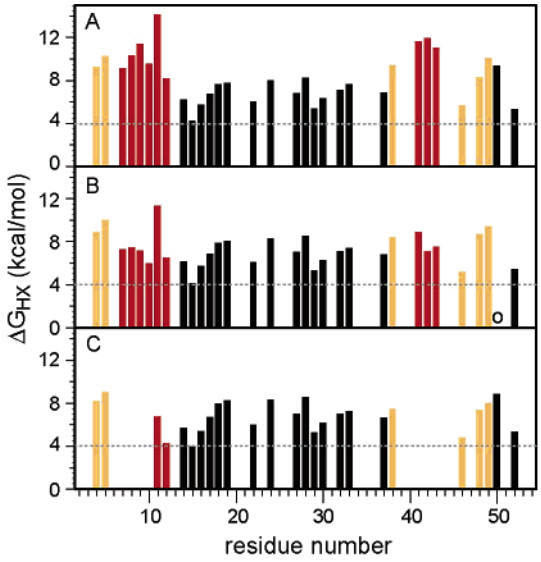

FIGURE 1: Apparent residue-specific conformational free energies of metal-substituted *Pf* A2K rubredoxin. Hydrogen exchange rate constants (k_{ex}) for Zn(II)-substituted (A), Ga(III)-substituted (B), and Ge(IV)-substituted (C) rubredoxin were converted to conformational equilibria values (k_1/k_2) assuming that the rate constants for the base-catalyzed chemical exchange step (k_3) are given by model peptide values (*62*). The free energy of the conformational opening transition was then derived from the formula $\Delta G_{HX} = -RT \ln(k_{ex}/k_3)$. Data for amides with exchange rates differing by a factor of at least 10 for each unit change in the charge of the metal site are colored red. Orange is used for data for residues that change by a factor of at least 2 for each unit charge change. The dotted line indicates the approximate lower bound of detection for amides which exchange too rapidly with bulk water deuterons to be analyzed by these NMR experiments. The absence of kinetic data for residue 50 in the Ga(III) form protein, resulting from spectral overlap, is indicated (o). The average experimental uncertainty in the log rate constants is estimated to be 0.11.

Ge(IV)-substituted *Pf* A2K rubredoxin at 23 °C, for pH values of 4.5−8.5 [4.5−7.5 for Ge(IV)]. For 33 of the 48 backbone amide protons, exchange rate constants were obtained for two or more metal forms. For each monitored amide, the exchange rate was found to become proportional to OH^- concentration as the pH was increased into the base catalysis regime (i.e., above pH ~5.5−6.5), as reported previously for the Zn(II) form of rubredoxin (*29*). This proportionality between k_{ex} and OH^- concentration indicates the establishment of a pre-equilibrium for the exchange-competent open conformation.

The residue-specific conformational free energy values (ΔG_{HX}) for these three metal forms (Figure 1) indicate that increasing the metal charge results in a dramatic decrease in the apparent conformational stability for the residues surrounding the two segments that contain the four metal-coordinated cysteines (Cys 6−Cys 9 and Cys 39−Cys 42). As much as a 4 kcal/mol decrease in the apparent residue-specific stabilities of ≥4 kcal/mol results from changing the charge on the metal site by a single unit. All of the most protected amides in Zn(II)-substituted rubredoxin lie within these two segments surrounding the metal-coordinated cysteines. Nearly all of these slowly exchanging amides of the Zn(II)-substituted protein exchange too rapidly to be detected in Ge(IV)-substituted *Pf* A2K rubredoxin. In marked contrast, for much of the rest of the protein, the exchange rates are virtually indistinguishable among the three metal site charge

FIGURE 2: Spatial distribution of the metal site charge-dependent differential hydrogen exchange in *Pf* A2K rubredoxin. The backbone of the X-ray structure (*63*) is colored red and orange for amides with exchange rate constants varying by at least a factor of 10 and a factor of 2, respectively, for each unit change in the charge of the metal site. Amides exhibiting exchange rates that are approximately metal site charge-independent are colored black. The residues which exchange too rapidly for detection as well as the five prolines lacking the amide resonance are colored gray. Similarly colored are residues Cys 6, Tyr 13, and Cys 39 which exchange too slowly under these conditions to yield rate constant estimates.

states. Hence, the amides which appear to be much more conformationally protected in the Zn(II) form also appear to be far less protected than the remainder of the protein when the Ge^{4+} ion is substituted. Those residues that are affected by the change in metal charge are distributed around the metal binding site (Figure 2).

Differential Stability of Oxidized and Reduced Rubredoxin. Given the close isomorphism between the X-ray structures of the Zn(II) and Ga(III) forms of *C. pasteurianum* rubredoxin (*23*), such a marked apparent regional destabilization of the native state upon metal substitution is striking. On the other hand, the X-ray structures of Fe(II) and Fe(III) cytochrome *c* are also quite similar (*33*), despite the fact that the conformation of oxidized cytochrome *c* has long been known to be markedly less stable than that of the reduced state (*34*). However, for both rubredoxin and cytochrome *c*, irreversibility considerations have complicated the direct measurement of the differential conformational stability of the oxidized and reduced states. The ~10 kcal/mol difference in conformational stability between ferro- and ferricytochrome *c* was ultimately determined indirectly via redox measurements on the unfolded protein (*35*, *36*) and subsequently verified calorimetrically (*37*).

Essentially all of the differential conformational stability between Fe(II) and Fe(III) cytochrome *c* arises from the enhanced water interactions with the Fe(III) heme in the unfolded state (*35*, *36*). Hence, native-state interactions for the oxidized versus reduced cytochromes do not significantly contribute to the differential conformational stability for the two redox forms. However, for rubredoxin, the increase in the metal charge serves to decrease the net charge in the active site as a result of the four coordinating thiolates so that the Ge(IV) cluster is neutral. This, in turn, suggests that the free energy cost of desolvation during protein folding should be greatest for the doubly charged Zn(II) coordination complex. Hence, this simple desolvation analysis predicts that if the more highly charged metal sites were to affect the relative stability of the rubredoxin native state, the effect would be opposite in direction to that implied by the residue-

Scheme 1: Thermodynamic Coupling of the Oxidation−Reduction Reaction and the Conformational Free Energy of Stability

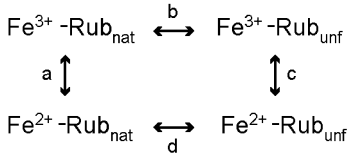

specific conformational stabilities derived from the hydrogen exchange data.

In the Born−Haber thermodynamic cycle (Scheme 1), the differential free energy of reduction in the native versus reversibly unfolded states ($\Delta G_a + \Delta G_c$) necessarily equals the negative of the differential conformational stability of the oxidized and reduced states ($\Delta G_b + \Delta G_d$). For the rubredoxins, the native-state redox reaction is the only branch of the cycle that has been directly measured near room temperature. In the absence of conditions for reversible unfolding of rubredoxin near ambient conditions, model compounds have been used to estimate the reduction potential of the protein in the unfolded state, which in turn allows prediction of the differential conformational stability of the redox states.

Although simple $Fe(SR)_4$ coordination complexes are often unstable in aqueous solution (*38*), coordination of Fe^{2+} and Fe^{3+} ions with excess β-mercaptoethanol anion in water yields a reduction potential of −0.35 V (*39*), similar to the −0.31 V potential of the native-state *Cp* rubredoxin (*40*) (standard calomel electrode reference). This 40 mV difference corresponds to a free energy difference of <1 kcal/mol. Furthermore, a set of peptide models based on the sequence for the second half of the pseudo-two-fold symmetric binding site of *Cp* rubredoxin (i.e., Cys-Pro-Leu-Cys-Gly-Val) yield reduction potentials in an aqueous micelle solution between −0.30 and −0.26 V (*41*). NMR analysis of these peptide complexes demonstrated not only the expected paramagnetically shifted Cys H^{β} resonances but also hydrogen bonding of the backbone amide protons to the metal-coordinated cysteine sulfur atoms (*42*), as seen in the native structure. The similarity between the native-state rubredoxin reduction potential and the reduction potential of these models for the unfolded-state complex indicates that there should be only a modest differential conformational stability between the Fe(II) and Fe(III) states of rubredoxin.

Distance Dependence of Differential Hydrogen Exchange. Interpreting these hydrogen exchange data in terms of metal charge-induced residue-specific conformational free energy appears to generate a conundrum. The most slowly exchanging region of the Zn(II) form of rubredoxin experiences a decrease in apparent stability of more than 8 kcal/mol upon Ge^{4+} substitution, yet the redox potential measurements (*41*) indicate no substantial alteration in the global conformational stability between the +2 and +3 metal charge states of rubredoxin. A more straightforward explanation can be obtained by reassessing the assumptions used to derive these residue-specific conformational free energy estimates. The exchange rates are proportionate to OH^- concentration over a range of pH near neutrality, consistent with pre-equilibration for the conformational opening transition. On the other hand, direct experimental evidence supporting the model peptide normalization assumption exists only for amides which exchange via a global unfolding pathway (*43*).

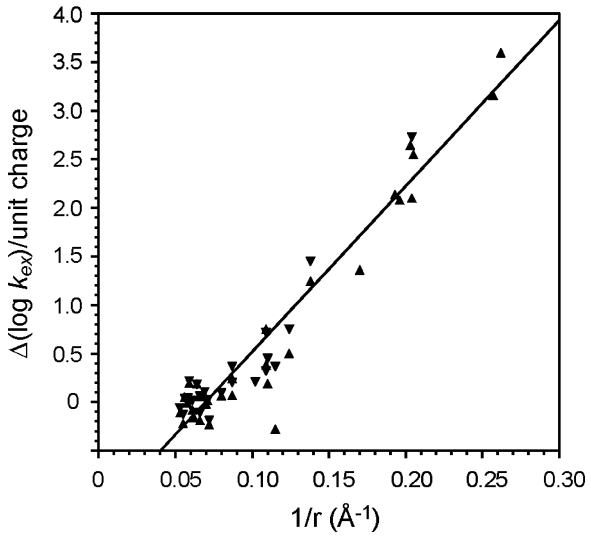

FIGURE 3: Distance dependence of the differential hydrogen exchange in metal-substituted *Pf* A2K rubredoxin. The log ratio of the base-catalyzed exchange rate constants for Zn(II)- vs Ga(III)-substituted *Pf* A2K rubredoxin (▲) is illustrated as a function of the inverse distance between the active site metal and the amide nitrogen. The analogous data for Zn(II)- vs Ge(IV)-substituted *Pf* A2K rubredoxin (▼) are normalized by a factor of 2 to reflect the differential metal site charge. The best-fit line predicts an effective uniform dielectric ϵ value of 15, assuming an electrostatic potential-induced variation of the amide nitrogen p*K* according to the relation $\epsilon_{eff} = 244/(r\Delta pK_a\Delta q)$, where r is the separation in angstroms and Δq is the change in charge (*63*).

It has long been recognized that electrostatic interactions can modulate protein hydrogen exchange kinetics (*44*−*48*). For the mechanistically simple base-catalyzed reaction, the rate of abstraction of the amide proton by hydroxide ion is directly dependent on the p*K* of that amide nitrogen which, in turn, is dependent on the stabilization of the amide anion intermediate by the local electrostatic field potential. Theoretical techniques, particularly continuum Poisson−Boltzmann modeling (*49*), have had some success at predicting acid−base p*K* shifts in protein surface residues due to variations in the electrostatic potential. Despite the comparatively low acidity of the amide group, the analogous dependence on the local electrostatic potential will apply.

The simplest model of a uniform dielectric environment yields the $1/r$ dependence for the electrostatic potential of Coulomb's Law. The log ratios of the base-catalyzed exchange rate constants for Zn(II)- versus Ga(III)-substituted *Pf* A2K rubredoxins were analyzed as a function of inverse distance to the metal (Figure 3). Close correlation to a linear dependence was observed for nearly all amides within 12 Å of the metal. A similar inverse distance dependence was observed for the log ratio of the hydrogen exchange rate constants with the Zn(II)- and Ge(IV)-substituted proteins, when normalized for the two unit charge difference (Figure 3). The exchange rate constant ratios for these residues span nearly 4 orders of magnitude. In contrast, for amides more than 12 Å from the metal, the exchange rates were comparatively insensitive to the charge of the metal site, indicating virtually no differential effect on the apparent conformational stability for the rest of the protein.

The fact that the Zn(II)- versus Ge(IV)-substituted *Pf* A2K rubredoxin data, normalized for the +2 charge change, closely follow the data from the Zn(II) versus Ga(III) form protein comparison indicates that the response is operationally linear with respect to the electrostatic potential. The only marked deviation from proportionality between the Zn(II) versus Ga(III) and Zn(II) versus Ge(IV) exchange data occurs at Tyr 11, for which the amide proton is hydrogen bonded to the metal-coordinated sulfur of Cys 9 [note that all other sulfur-bonded amide protons exchange too rapidly in Ge(IV)-substituted *Pf* A2K rubredoxin to be detected]. The nonlinear behavior for the amide of Tyr 11 may reflect the limitations of assuming that the differential charge lies exclusively on the metal for the $1/r$ calculation, when in fact electron density transfers to the metal from the covalently bound sulfurs. Given the nearly tetrahedral arrangement of the metal cluster, this point charge approximation will rapidly become more accurate as the amide−metal distance increases. However, the Tyr 11 amide proton that is directly hydrogen bonded to a bridging sulfur will surely be more sensitive to electron density redistribution along the metal−sulfur bond as a function of the metal charge.

There are 23 other amides for which exchange data were obtained on all three metal forms. For all but one of these residues, the differential exchange rates for the Zn(II)- versus Ge(IV)-substituted *Pf* A2K rubredoxin agree with those of the Zn(II) versus Ga(III) form proteins to within an rmsd of $10^{0.11}$ (a factor of 30%). This value provides an upper boundary for the experimental uncertainty of the independent data sets being compared. It also provides an independent test with regard to the linearity of the assumed electrostatic effects and of any structural variation among the three metal form proteins.

Interpreting these differential exchange kinetics in terms of shifts in the p*K* values of the amide nitrogens allows an effective dielectric constant value ϵ of 15 to be derived from the slope of the best-fit line (Figure 3). This effective ϵ value is intermediate between the bulk water dielectric of 80 and the low ϵ values that are commonly assumed for the protein interior in continuum electrostatics analysis (*49*). The residual deviations from the best-fit line between the differential log exchange rate constants and the inverse distance to the metal generally exceed the experimental uncertainty. Much of this residual deviation likely results from the overly simplistic assumption of a uniform dielectric, indicating that these data may serve to monitor systematic variations of the effective dielectric sensed at each amide nitrogen.

The effective dielectric constant derived from these hydrogen exchange measurements can be expected to exceed the value that is directly estimated from the native-state structure, since at minimum one water molecule, and more likely a chain of water molecules (*50*), must contact the amide hydrogen to effect base-catalyzed exchange. The effective dielectric constant observed for the *Pf* A2K rubredoxin exchange is well below that of the bulk water phase, indicating that the chemical exchange step does not occur from a conformational state that is adequately represented by a fully hydrated free peptide.

DISCUSSION

Application of the peptide normalization protocol to the hydrogen exchange data of the metal-substituted *Pf* A2K rubredoxins yields a severely erroneous estimate of the differential local conformational stability among these proteins. The electrostatic potential-dependent variations in the hydrogen exchange rates account for a large proportion of the total apparent protection for many of the most slowly exchanging amides in the most thermostable protein characterized to date. As discussed below, the ϵ value of 15 obtained in this study is not atypical of previous estimates of the effective dielectric constants within the protein interior, suggesting that comparable electrostatic potential-dependent variations should be anticipated in other proteins for exchange reactions that occur via local conformational fluctuations. On the other hand, direct experimental measurement of the electrostatic potential at a specific position within a protein interior is problematic, so a quantitative comparison to the rubredoxin system is not straightforward. However, in certain cases, direct determination of the local electric field gradient within a protein interior has proven to be feasible. The Stark effect has been monitored in the bacterial photosynthetic reaction center to measure how the electric field that is induced by the charge separation between the Q_A quinone and the bacteriochlorophyll special pair shifts the absorption of the bacteriopheophytin and the intervening bacteriochlorophyll monomer (*51*). The electric field at these two chromophores along each of the two branches in the photosynthetic complex ranges from 2.4 to 5.1×10^6 V/cm. An analogous Stark effect on the vibrational spectra of carbon monoxide has been used to determine an electric field intensity of 1×10^7 V/cm within the Xe 4 internal cavity of myoglobin (*52*). As deduced from the rubredoxin data of Figure 3, the difference in electrostatic potential for amides that are 4 and 8 Å from the metal predicts an electric field intensity of 2.8×10^6 V/cm. Although *Pf* rubredoxin is exceptionally well suited for deconvolution of the contributions from electrostatic interactions and conformational equilibria to the observed hydrogen exchange data, the occurrence of electrostatic interactions of comparable intensity in other proteins indicates that residual conformation-dependent modulation of chemical exchange rate constant k_3 must be more generally anticipated.

Changes in surface charge have long been known to shift the pH value at which protein amides exchange most slowly (*45*, *46*). However, it is not always straightforward to determine whether this effect results from an electrostatic potential-dependent shifting of the H^+- versus OH^--catalyzed intrinsic chemical rate constants rather than from a pH-dependent change in conformational stability. Solvent-exposed amides on protein surfaces and in model α-helical peptides have been observed to exchange up to 20-fold faster (*53*−*55*) as well as comparably slower (*45*, *55*) than their reference peptide values, despite the absence of any apparent conformational opening transition being required. Such conformation-dependent perturbations from ideal peptide exchange kinetics can be expected only to be increased for more buried amide sites which are less solvated in their exchange-competent state.

Even application of the peptide normalization assumption to the estimation of protein thermodynamic global stability based on the exchange behavior of the most protected amides can warrant circumspection as the effects of conformation-dependent variation of the electrostatic potential have previously been observed in the unfolded state. Non-nearest

neighbor charge−charge interactions cause p*K* shifts of at least 0.5 pH unit for side chain carboxylates of an unfolded SH3 domain (*56*). Similar electrostatic potential variations at the backbone amide nitrogens must necessarily result in comparable shifts of their p*K* values.

Electrostatic potential variations are by no means the only mechanism by which chemical exchange rate constant k_3 can be altered from model peptide values by residual conformational structure. The amide nitrogen p*K* value is also known to depend on the local backbone torsion angles (*57*). The lack of conformational averaging of those angles due to the presence of residual structure will yield p*K* values differing from those of a flexible model peptide. In addition, steric hindrance to complete solvation of the amide group is known to alter the hydrogen exchange behavior even in simple model dipeptide studies (*58*). Such effects will further contribute to the differential ionization behavior of the backbone amides when larger-scale residual conformational structure is present.

The differential exchange rate constants resulting from a change in the metal site charge correlate closely with the reciprocal of the distances between the amide nitrogens and the metal in the X-ray structure. These results strongly indicate that the exchange-competent conformations retain significant resemblance to the native structure. A measure of the preservation of nativelike structure in the exchange-competent state can be drawn from the data of Figure 3. Although the deviations from the best-fit line may largely reflect local variations in the effective dielectric constant, a complementary analysis can be based on the assumption of a purely uniform dielectric and that all of the experimental deviations from the best-fit line arise solely from variations in the amide nitrogen−metal distances relative to those of the reference X-ray structure. The apparent distance between the amide nitrogen and the metal in the exchange-competent state can then be estimated by adjusting the distance for each residue to match the best-fit line. This analysis predicts a median difference of only 0.6 Å in the nitrogen−metal distance as compared to the X-ray coordinates for all of the amides within 12 Å of the metal. This estimate approximates an upper bound to the radial displacement from the metal which occurs in the transition to the exchange-competent state. For a given amide to maintain the same observed electrical potential effect on the hydrogen exchange, a larger increase in distance from the metal must be complemented by a decreased effective dielectric constant, while an increased ϵ value would be required for amides which move closer to the metal during the hydrogen exchange transition. This correlation implies a distance dependence of the effective dielectric constant which is the opposite of what is normally expected.

A particular case in point regarding the preservation of nativelike structure in the exchange-competent state is that of residue Phe 49. In the X-ray structure of *Pf* rubredoxin (*59*), the distance between the Phe 49 amide nitrogen and the metal is just more than 8 Å, which is closer than the corresponding distance for either residue 48 or 50. The average differential exchange rates of the Zn(II) versus Ga(III) and Zn(II) versus Ge(IV) data for residue Phe 49 of *Pf* A2K rubredoxin indicate a 4-fold increase in rate for each unit change in the charge of the metal site. A correspondingly smaller effect is observed for the more distant amides of residues 48 and 50. This 4-fold increase in rate per unit change in metal site charge is far higher than that anticipated from a local unfolding model. The dielectric value of 80 for the bulk water exchange assumed in the local unfolding model would markedly decrease the electrostatic field potential effect of the metal site charge that is sensed by the Phe 49 amide nitrogen. Furthermore, any loss of nativelike conformation for the backbone segment separating the Phe 49 amide from the metal would tend to increase their interatomic distance. Twenty-three covalent bonds separate the amide nitrogen of Phe 49 from the metal via the side chain of Cys 42. If the peptide segment between Cys 42 and Phe 49 were to adopt a random coil-type conformation in the exchange-competent state, the distance between these two atoms could be expected to be 2−3-fold larger than the distance shown by the X-ray structure with a corresponding smaller electrostatic potential effect.

The hyperthermophile rubredoxin from *P. furiosus* offers an excellent model system for analyzing the effects of electrostatic potential on hydrogen exchange which occur via small-scale conformational fluctuations. Rubredoxin is the only system for which the diamagnetic metal charge state in a protein binding site has been varied from +2 to +4 with a reference structure known to 1 Å resolution (*30*). Of the slowly exchanging amides of *Pf* rubredoxin, only Cys 6 exhibits denaturant-dependent hydrogen exchange rates for guanidinium chloride concentrations of <1 M at 60 °C (*28*), indicating that small-scale conformational fluctuations dominate much of the hydrogen exchange behavior at temperatures well below the protein T_m value of 144 °C (*21*).

The hydrogen exchange behavior for two-thirds of the backbone amides can be readily monitored by the conventional ^2H_2O exchange protocol in two or more metal site charge states. Changing the metal site charge appears to have only a small effect on the global conformational stability and no apparent discernible effect on the nonglobal conformational transitions that give rise to the hydrogen exchange kinetics monitored in this study. This interpretation is reinforced by ab initio unrestricted Hartree−Fock calculations on the Fe(II) and Fe(III) forms of the structurally homologous *C. pasteurianum* rubredoxin which indicate that little change occurs in the interactions between the metal site and the surrounding protein, and thus, the structure and electric field arising from the surrounding protein do not appreciably change upon reduction (*60*). As a result, the differential hydrogen exchange rates, which vary by up to $\sim 10^6$-fold as a function of metal site charge state, appear to arise nearly exclusively by variation of the intrinsic k_3 exchange rate constant due to the electrostatic potential-dependent alteration in the p*K* values of the backbone amide nitrogens.

Most of the earliest protein electrostatic calculations assumed a simple two-phase model of a weakly polarizable protein with a dielectric constant of 2−4 surrounded by a bulk aqueous phase (*61*). Although the desirability of directly modeling the more heterogeneous dielectric character of the protein structure was discussed (*62*), the experimental basis against which to test such models has often consisted of one or a few structurally perturbed side chain p*K* values (e.g., refs *63*−*66*) so that a freely adjustable ϵ value for the protein phase often proves sufficient to fit the data. When dielectric constant optimization is carried out on a large set of proteins

with shifted p*K* values from charged residues exhibiting a range of exposure to bulk solvent, a much higher value of ~20 is obtained (*67*). The primary contribution to this high polarizability of the protein is believed to arise from the mobile charged side chains on the protein surface that can effectively shield electrostatic interactions near the aqueous interface but are less efficient at shielding structurally buried interactions (*68*). This observation has given rise to three-phase models which include a low internal dielectric and a protein surface boundary region having an ϵ value of 20−30 (*69*, *70*).

As the dielectric contribution of dynamic conformational reorientation has become more explicitly considered, the inherent incompatibility between the dielectric constant approximation and the standard atomic force fields used for molecular dynamics calculations becomes more apparent. These nonpolarizable force fields are optimized for $\epsilon = 1$ conditions with the internal fixed charge distributions being hyperpolarized to model the average dielectric susceptibility interactions in the bulk phase. Polarizable force fields (*71*) appear to offer a promising means of directly modeling the electrostatic forces within the protein in a self-consistent fashion. Using such calculations to interpret the detailed hydrogen exchange kinetics may aid in overcoming the pessimism expressed by Hvidt regarding the value of these measurements in the absence of the peptide normalization assumption (*2*). The large number of structurally buried amide nitrogen p*K* shifts described in this work should provide a valuable experimental basis for testing such approaches. The small size and the availability of high-resolution structures for various rubredoxins will facilitate these efforts.

ACKNOWLEDGMENT

We acknowledge the use of the Wadsworth Center NMR facility and the technical assistance of Lynn McNaughton.

SUPPORTING INFORMATION AVAILABLE

A table containing the differential base-catalyzed hydrogen exchange rate constants at 23 °C for each monitored residue in the Zn(II)-, Ga(III)-, and Ge(IV)-substituted *Pf* A2K rubredoxins. This material is available free of charge via the Internet at http://pubs.acs.org.

REFERENCES

1. Hvidt, A., and Linderstrøm-Lang, K. (1954) Exchange of hydrogen atoms in insulin with deuterium atoms in aqueous solutions, *Biochim. Biophys. Acta 14*, 574−575.
2. Hvidt, A., and Nielsen, S. O. (1966) Hydrogen Exchange in Proteins, *Adv. Protein Chem. 21*, 287−386.
3. Englander, S. W. (1967) Hydrogen exchange, in *Poly-a-amino acids* (Fasman, G., Ed.) pp 339−367, Marcel Dekker, Inc., New York.
4. Woodward, C. K., and Rosenberg, A. (1971) Studies of hydrogen exchange in proteins, *J. Biol. Chem. 246*, 4114−4120.
5. Mayo, S. L., and Baldwin, R. L. (1993) Guanidinium chloride induction of partial unfolding in the amide proton exchange in RNase A, *Science 262*, 873−876.
6. Swint-Kruse, L., and Robertson, A. D. (1996) Temperature and pH dependence of hydrogen exchange and global stability for ovomucoid third domain, *Biochemistry 35*, 171−180.
7. Yi, Q., Scalley, M. L., Simons, K. T., Gladwin, S., and Baker, D. (1997) Characterization of the free energy spectrum of peptostreptococcal protein L, *Fold. Des. 2*, 271−280.
8. Alexandrescu, A. T., Jaravine, V. A., Dames, S. A., and Lamour, F. P. (1999) NMR hydrogen exchange of the OB-fold protein LysN as a function of denaturant: The most conserved elements of structure are the most stable to unfolding, *J. Mol. Biol. 289*, 1041−1054.
9. Itzhaki, L. S., Neira, J. L., and Fersht, A. R. (1997) Hydrogen exchange in chymotrypsin inhibitor 2 probed by denaturants and temperature, *J. Mol. Biol. 270*, 88−89.
10. Neira, J. L., Sevilla, P., Menéndez, M., Bruix, M., and Rico, M. (1999) Hydrogen exchange in ribonuclease A and ribonuclease S: Evidence for residual structure in the unfolded state under native conditions, *J. Mol. Biol. 285*, 627−643.
11. Huyghes-Despointes, B. M., Pace, C. N., Englander, S. W., and Scholtz, J. M. (2001) Measuring the conformational stability of a protein by hydrogen exchange, *Methods Mol. Biol. 168*, 69−92.
12. Schoenborn, B. P., Hanson, J. C., Darling, G. D., and Norvell, J. C. (1978) Real space refinement of neutron diffraction data from carbon monoxide sperm whale myoglobin, *Acta Crystallogr. A34*, 65.
13. Tüchsen, E., Hvidt, A., and Ottesen, M. (1980) Enzymes immobilized as crystals. Hydrogen isotope exchange of crystalline lysozyme, *Biochimie 62*, 563−566.
14. Kossiakoff, A. A. (1982) Protein dynamics investigated by the neutron diffraction-hydrogen exchange technique, *Nature 296*, 713−721.
15. Wlodawer, A., and Sjolin, L. (1982) Hydrogen exchange in ribonuclease A: Neutron diffraction study, *Proc. Natl. Acad. Sci. U.S.A. 79*, 1418−1422.
16. Woodward, C. K., Ellis, L. M., and Rosenberg, A. (1975) Solvent accessibility in folded proteins: Studies of hydrogen exchange in trypsin, *J. Biol. Chem. 250*, 432−439.
17. Dixon, M. E., Hitchens, T. K., and Bryant, R. G. (2000) Comparison of pressure and temperature activation parameters for amide hydrogen exchange in T4 lysozyme, *Biochemistry 39*, 248−254.
18. Krishna, M. M. G., Hoang, L., Lin, Y., and Englander, S. W. (2004) Hydrogen exchange methods to study protein folding, *Methods 34*, 51−64.
19. Bai, Y., Sosnick, T. R., Mayne, L., and Englander, S. W. (1995) Protein folding intermediates: Native-state hydrogen exchange, *Science 269*, 192−197.
20. Hernández, G., and LeMaster, D. M. (2001) Reduced temperature dependence of collective conformational opening in a hyperthermophile rubredoxin, *Biochemistry 40*, 14384−14391.
21. LeMaster, D. M., Tang, J., and Hernández, G. (2004) Absence of Kinetic Thermal Stabilization in a Hyperthermophile Rubredoxin Indicated by 40 Microsecond Folding in the Presence of Irreversible Denaturation, *Proteins 57*, 118−127.
22. Moura, I., Teixeira, M., LeGall, J., and Moura, J. J. (1991) Spectroscopic studies of cobalt and nickel substituted rubredoxin and desulforedoxin, *J. Inorg. Biochem. 44*, 127−139.
23. Maher, M., Cross, M., Wilce, M. C. J., Guss, J. M., and Wedd, A. G. (2004) Metal-substituted derivatives of the rubredoxin from *Clostridium pasteurianum*, *Acta Crystallogr. D60*, 298−303.
24. Hwang, T. L., vanZijl, P. C. M., and Mori, S. (1998) Accurate Quantitation of Water-Amide Proton Exchange Rates using the Phase-Modulated CLEAN chemical EXchange (CLEANEX-PM) Approach with a Fast-HSQC (FHSQC) Detection Scheme, *J. Biomol. NMR 11*, 221−226.
25. Min, T., Ergenekan, C. E., Eidsness, M. K., Ichiye, T., and Kang, C. (2001) Leucine 41 is a Gate for Water Entry in the Reduction of *Clostridium pasteurianum* Rubredoxin, *Protein Sci. 10*, 613−621.
26. Blake, P. R., Park, J. B., Zhou, Z. H., Hare, D. R., Adams, M. W. W., and Summers, M. F. (1992) Solution-state Structure by NMR of Zinc-substituted Rubredoxin from the Marine Hyperthermophilic Archaebacterium *Pyrococcus furiosus*, *Protein Sci. 1*, 1508−1521.
27. Richie, K. A., Teng, Q., Elkin, C. J., and Kurtz, D. M. (1996) 2D ^{1}H and 3D ^{1}H-^{15}N NMR of Zinc-rubredoxins: Contributions of the β-Sheet to Thermostability, *Protein Sci. 5*, 883−894.
28. Hiller, R., Zhou, Z. H., Adams, M. W. W., and Englander, S. W. (1997) Stability and dynamics in a hyperthermophilic protein with melting temperature close to 200 °C, *Proc. Natl. Acad. Sci. U.S.A. 94*, 11329−11332.
29. Hernández, G., Jenney, F. E., Adams, M. W. W., and LeMaster, D. M. (2000) Millisecond time scale conformational flexibility in a hyperthermophile protein at ambient temperature, *Proc. Natl. Acad. Sci. U.S.A. 97*, 3166−3170.

30. LeMaster, D. M., Minnich, M., Parsons, P. J., Anderson, J. S., and Hernández, G. (2006) Tetrathiolate coordination of germanium(IV) in a protein active site, *J. Inorg. Biochem. 100*, 1410−1412.
31. Cavagnero, S., Zhou, Z. H., Adams, M. W. W., and Chan, S. I. (1998) Unfolding mechanism of rubredoxin from *Pyrococcus furiosus*, *Biochemistry 37*, 3377−3385.
32. Bonomi, F., Fessas, D., Iametti, S., Kurtz, D. M., and Mazzini, S. (2000) Thermal stability of *Clostridium pasteurianum* rubredoxin: Deconvoluting the contributions of the metal site and the protein, *Protein Sci. 9*, 2413−2426.
33. Takano, T., and Dickerson, R. E. (1981) Conformation change of cytochrome *c*. II. Ferricytochrome *c* refinement at 1.8 Å and comparison with the ferrocytochrome structure, *J. Mol. Biol. 153*, 95−115.
34. Butt, W. D., and Keilin, D. (1962) Absorption spectra and some other properties of cytochrome *c* and of its compounds with ligands, *Proc. R. Soc. London, Ser. B 156*, 429−458.
35. Bixler, J., Bakker, G., and McLendon, G. (1992) Electrochemical Probes of Protein Folding, *J. Am. Chem. Soc. 114*, 6938−6939.
36. Hilgen-Willis, S., Bowden, E. F., and Pielak, G. J. (1993) Dramatic stabilization of ferricytochrome-*c* upon reduction, *J. Inorg. Biochem. 51*, 649−653.
37. Cohen, D. S., and Pielak, G. J. (1995) Entropic stabilization of cytochrome *c* upon reduction, *J. Am. Chem. Soc. 117*, 1675−1677.
38. Rao, P. V., and Holm, R. H. (2004) Synthetic Analogues of Active Sites of Iron−Sulfur Proteins, *Chem. Rev. 104*, 527−559.
39. Werth, M. T., Kurtz, D. M., Jr., Howes, B. D., and Huynh, B. H. (1989) Observation of S=2 EPR Signals from Ferrous Iron-Thiolate Complexes. Relevance to Rubredoxin-Type Sites in Proteins, *Inorg. Chem. 28*, 1357−1361.
40. Eaton, W. A., and Lovenberg, W. (1973) in *Iron−sulfur Proteins* (Lovenberg, W., Ed.) Vol. 2, p 131, Academic Press, New York.
41. Sun, W. Y., Ueyama, N., and Nakamura, A. (1998) Electrochemical mimicking of reduced rubredoxin by iron(II) complexes of cysteine peptide thiolate in aqueous micelle solution, *J. Electroanal. Chem. 448*, 105−109.
42. Sun, W. Y., Ueyama, N., and Nakamura, A. (1998) Stabilization of Hydrolytically Labile Iron(II)-Cysteine Peptide Thiolate Complexes in Aqueous Triton X-100 Micelle Solution: Spectroscopic Properties Mimicking of Reduced Rubredoxin, *Biopolymers 46*, 1−10.
43. Miller, D. W., and Dill, K. A. (1995) A statistical mechanical model for hydrogen exchange in globular proteins, *Protein Sci. 4*, 1860−1873.
44. Kim, P. S., and Baldwin, R. L. (1982) Influence of Charge on the Rate of Amide Proton Exchange, *Biochemistry 21*, 1−5.
45. Tüchsen, E., and Woodward, C. (1985) Hydrogen Kinetics of Peptide Amide Protons at the Bovine Pancreatic Trypsin Inhibitor Protein−Solvent Interface, *J. Mol. Biol. 185*, 405−419.
46. Delepierre, M., Dobson, C. M., Karplus, M., Poulsen, F. M., States, D. J., and Wedin, R. E. (1987) Electrostatic Effects and Hydrogen Exchange Behavior in Proteins. The pH Dependence of Exchange Rates in Lysozyme, *J. Mol. Biol. 197*, 111−130.
47. Dempsey, C. E. (1988) pH Dependence of Hydrogen Exchange from Backbone Peptide Amides of Melittin in Methanol, *Biochemistry 27*, 6893−6901.
48. Fogolari, F., Esposito, G., Vigino, P., Briggs, J. M., and McCammon, J. A. (1998) pK_a Shift Effects on Backbone Amide Base-Catalyzed Hydrogen Exchange Rates in Peptides, *J. Am. Chem. Soc. 120*, 3735−3738.
49. Honig, B., and Nicholls, A. (1995) Classical Electrostatics in Biology and Chemistry, *Science 268*, 1144−1149.
50. Damjanovic, A., Garcia-Moreno, B., Lattman, E. E., and Garcia, A. E. (2005) Molecular Dynamics Study of Water Penetration in Staphyloccocal Nuclease, *Proteins 60*, 433−449.
51. Steffen, M. A., Lao, K., and Boxer, S. G. (1994) Dielectric Asymmetry in the Photosynthetic Reaction Center, *Science 264*, 810−816.
52. Kriegl, J. M., Nienhaus, K., Deng, P. C., Fuchs, J., and Nienhaus, G. U. (2003) Ligand dynamics in a protein internal cavity, *Proc. Natl. Acad. Sci. U.S.A. 100*, 7069−7074.
53. Rohl, C. A., and Baldwin, R. L. (1994) Exchange kinetics of individual amide protons in ^{15}N-labeled helical peptides measured by isotope-edited NMR, *Biochemistry 33*, 7760−7767.
54. Dempsey, C. E. (1995) Hydrogen bond stabilities in the isolated alamethicin helix, *J. Am. Chem. Soc. 117*, 7526−7534.
55. Mori, S., Abeygunawardana, C., Berg, J. M., and vanZijl, P. C. M. (1997) NMR study of rapidly exchanging backbone amide protons in staphylococcal nuclease and the correlation with structural and dynamic properties, *J. Am. Chem. Soc. 119*, 6844−6852.
56. Tollinger, M., Crowhurst, K. A., Kay, L. E., and Forman-Kay, J. D. (2003) Site-specific contributions to the pH dependence of protein stability, *Proc. Natl. Acad. Sci. U.S.A. 100*, 4545−4550.
57. Radkiewicz, J. L., Zipse, H., Clarke, S., and Houk, K. N. (2001) Neighboring side chain effects on asparaginyl and aspartyl degradation: An ab initio study of the relationship between peptide conformation and backbone NH acidity, *J. Am. Chem. Soc. 123*, 3499−3506.
58. Bai, Y. W., Milne, J. S., Mayne, L., and Englander, S. W. (1993) Primary structure effects on peptide group hydrogen-exchange, *Proteins 17*, 75−86.
59. Bau, R., Rees, D. C., Kurtz, D. M., Scott, R. A., Huang, H. S., Adams, M. W. W., and Eidsness, M. K. (1998) Crystal-structure of rubredoxin from *Pyrococcus furiosus* at 0.95 Angstrom resolution, and the structures of N-terminal methionine and formylmethionine variants of *Pf* Rd. Contributions of N-terminal interactions to thermostability, *J. Biol. Inorg. Chem. 3*, 484−493.
60. Beck, B. W., Koerner, J. B., and Ichiye, T. (1999) Ab Initio Quantum Mechanical Study of Metal Substitutions in Analogues of Rubredoxin: Implication for Redox Potential Control, *J. Phys. Chem. B 103*, 8006−8015.
61. Sharp, K. A., and Honig, B. (1990) Electrostatic Interactions in Macromolecules: Theory and Applications, *Annu. Rev. Biochem. 19*, 301−332.
62. Warshel, A., and Russell, S. T. (1984) Calculations of electrostatic interactions in biological systems and in solutions, *Q. Rev. Biophys. 17*, 283−422.
63. Rees, D. C. (1980) Experimental evaluation of the effective dielectric constant of proteins, *J. Mol. Biol. 141*, 323−326.
64. Sternberg, M. J. E., Hayes, F. R. F., Russell, A. J., Thomas, P. G., and Fersht, A. R. (1987) Prediction of electrostatic effects of engineering of protein charges, *Nature 330*, 86−88.
65. Langsetmo, K., Fuchs, J. A., Woodward, C., and Sharp, K. A. (1991) Linkage of thioredoxin stability to titration of ionizable groups with perturbed pK_a, *Biochemistry 30*, 7609−7614.
66. Garcia-Moreno, B., Dwyer, J. J., Gittis, A. G., Lattman, E. E., Spencer, D. S., and Stites, W. E. (1997) Experimental Measurement of the Effective Dielectric in the Hydrophobic Core of a Protein, *Biophys. Chem. 64*, 211−224.
67. Antosiewicz, J., McCammon, J., and Gilson, M. (1994) Prediction of pH dependent properties of proteins, *J. Mol. Biol. 238*, 415−436.
68. Simonson, T., and Perahia, D. (1995) Internal and interfacial dielectric properties of cytochrome *c* from molecular dynamics in aqueous solution, *Proc. Natl. Acad. Sci. U.S.A. 92*, 1082−1086.
69. Furuki, T., Sakurai, M., and Inoue, Y. (1995) Multidielectric description of electrostatic environment surrounding a bound substrate in enzymic systems, *J. Phys. Chem. 99*, 12047−12053.
70. Hofinger, S., and Simonson, T. (2001) Dielectric relaxation in proteins: A continuum electrostatics model incorporating dielectric heterogeneity of the protein and time-dependent charges, *J. Comput. Chem. 22*, 290−305.
71. Ponder, J. W., and Case, D. A. (2003) Force fields for protein simulations, *Adv. Protein Chem. 66*, 27−85.

BI0605540